Supplement of Atmos. Chem. Phys., 25, 6407–6428, 2025
https://doi.org/10.5194/acp-25-6407-2025-supplement

Atmospheric Chemistry and Physics
Open Access
EGU

Supplement of

Spectral optical properties of soot: laboratory investigation of propane flame particles and their link to composition

Johannes Heuser et al.

Correspondence to: Johannes Heuser (johannes.heuser@lisa.ipsl.fr) and Claudia Di Biagio (claudia.dibiagio@lisa.ipsl.fr)

Figure S1. Absorption coefficient calculated at 450 and 630 nm with the extinction-minus-scattering method (EMS) compared to the filter-based values of the PP_UniMI, MWAA, and the MAAP for all CESAM experiments on CS. For comparison purposes, the EMS and MAAP online measurements are averaged over the PP_UniMI and MWAA sampling times (15 to 120 min for the different experiments). The b_{abs} values from the MWAA are interpolated at 450 based on the Absorption Ångström Exponent (AAE) calculated as the power-law fit of b_{abs} vs the wavelength ($b_{abs} \sim \lambda^{-AAE}$) while the PP_UniMI original data at 448 nm are taken. For comparison at 630 nm, the MAAP data at 637 nm and the MWAA and PP_UniMI data at 635 nm are considered. A linear fit of the relation between the measurements of the two stiles was calculated with an assumed intercept at zero and added in red together with a 95 % confidence interval of the fit. The correlation coefficient (R^2) for the fit is also indicated.

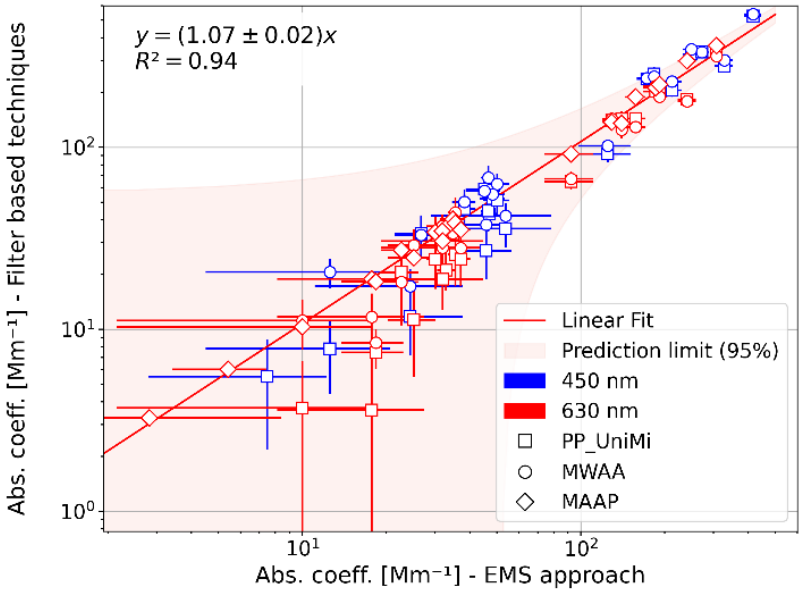

Figure S2. Example illustrating the statistical analysis performed on MAC measurements. a) Gaussians probability (Eq. 7) stacking of measured MAC values. Data shown correspond to CS1 observations. S1b) shows the total ensemble of PDFs for all measured CS1 MAC values. The text on top of the figure reports the number of soot generations corresponding to CS1 analysis, in this case 13 (Gen.=13), and the number of single 3-minute MAC observations in the ensemble of experiments (n=600, which are stacked with a resolution of 0.01 m^2g^{-1} and shown in b). S1a) shows then the sum of all Gaussians in b) and fitted Gaussians distribution to the sum of all Gaussian values providing the count median supplied in the header of the graphic.

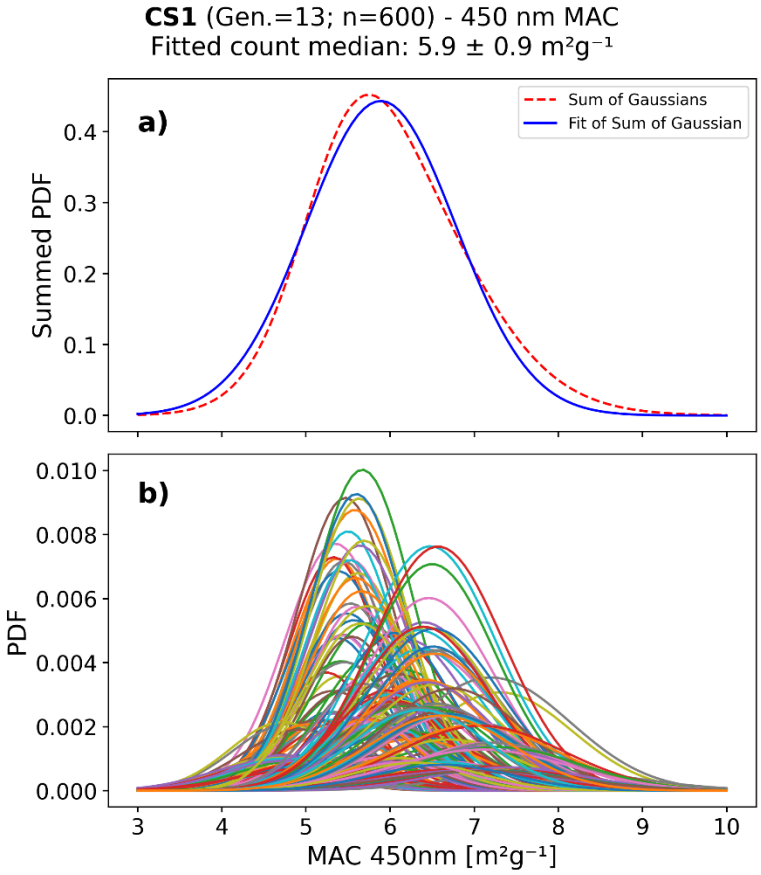

Figure S3. Equivalent plot to Fig. 3, illustrating the results at 630nm: Sum of Gaussians of MAC/MSC/MEC values and fitted Gaussians distribution of the sum for CS1 to CS5 at 630 nm. For each plot the soot, together with their number of generations, and used data points (n) is given. Further, the mean value of the peak together with its standard deviation is provided, determined from the fit of Eq. (7).

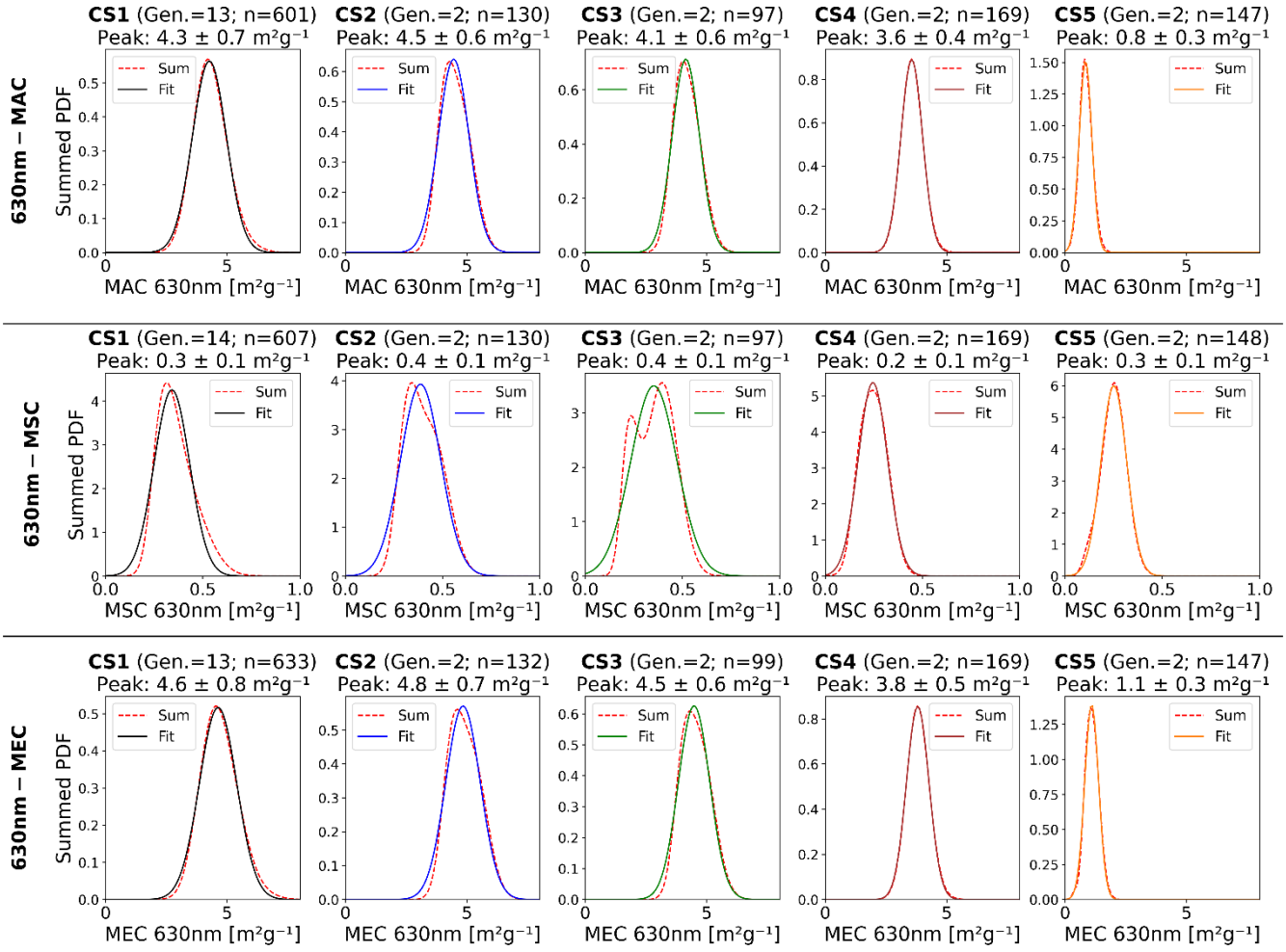

Figure S4. Equivalent plot to Fig. 6, illustrating the results in relation to the EC/OC ratio: Compositional dependent absorption mass absorption cross sections and its spectral variability represented by the AAE. The MAC data obtained in the present study at 550 nm (black points) are combined with observations from past literature and put in relation to the EC/OC soot content. Data retrieved as described for Fig.6. The EC/OC ratios, if not available from the original publication, were determined using EC+OC=TC assumption, thus $\frac{OC}{TC} = 1 - \frac{EC}{TC}$, and $\frac{EC}{OC} = \frac{EC}{TC}\frac{TC}{OC}$. In case no uncertainties for EC, OC, or TC were given, the EC/TC uncertainty was assumed to be true for OC/TC and then propagated (resulting in potential underestimations of the EC/OC uncertainty).

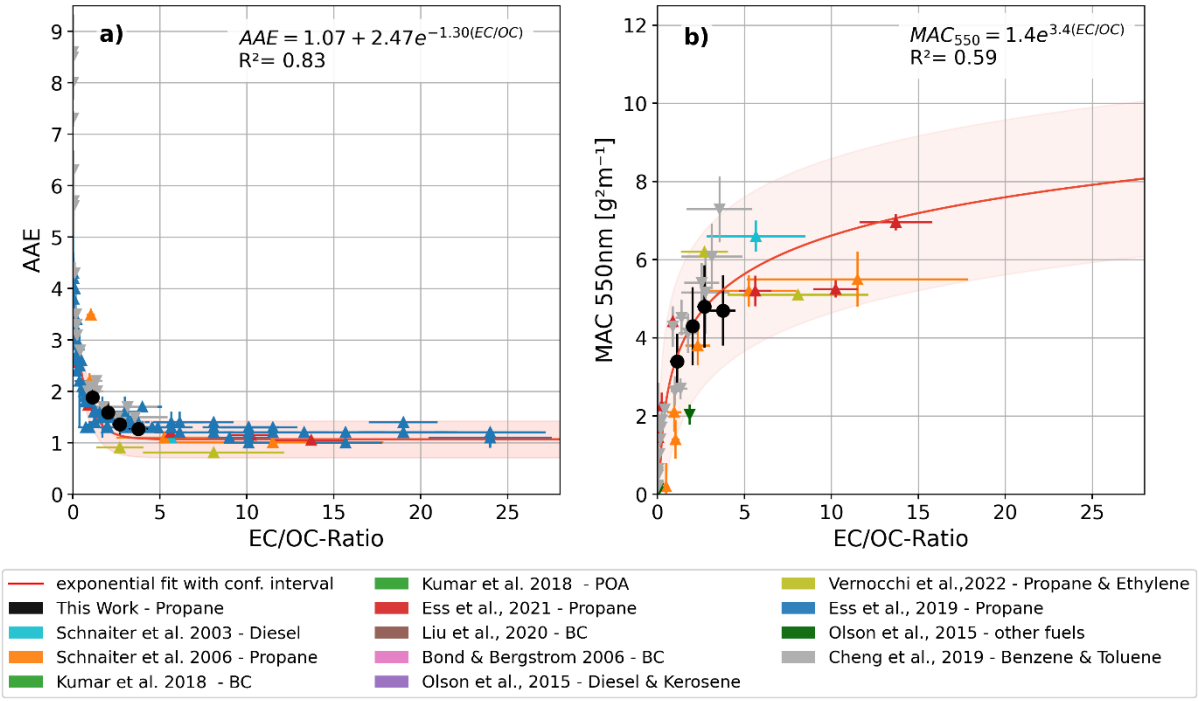

Figure S5. Additional plot to Fig. 6 with the scattering properties, illustrating the results in relation to the EC/TC ratio: Compositional dependent scattering mass absorption cross section and its spectral variability represented by the SAE. The MSC data obtained in the present study at 550 nm (black points) are combined with observations from past literature and put in relation to the EC/TC soot content. Data are fitted with the equation : $\boldsymbol{y = a + b * e^{(c*EC/TC)}}$. Please note that these identified relationships have only limited relevance as scattering depends on size.

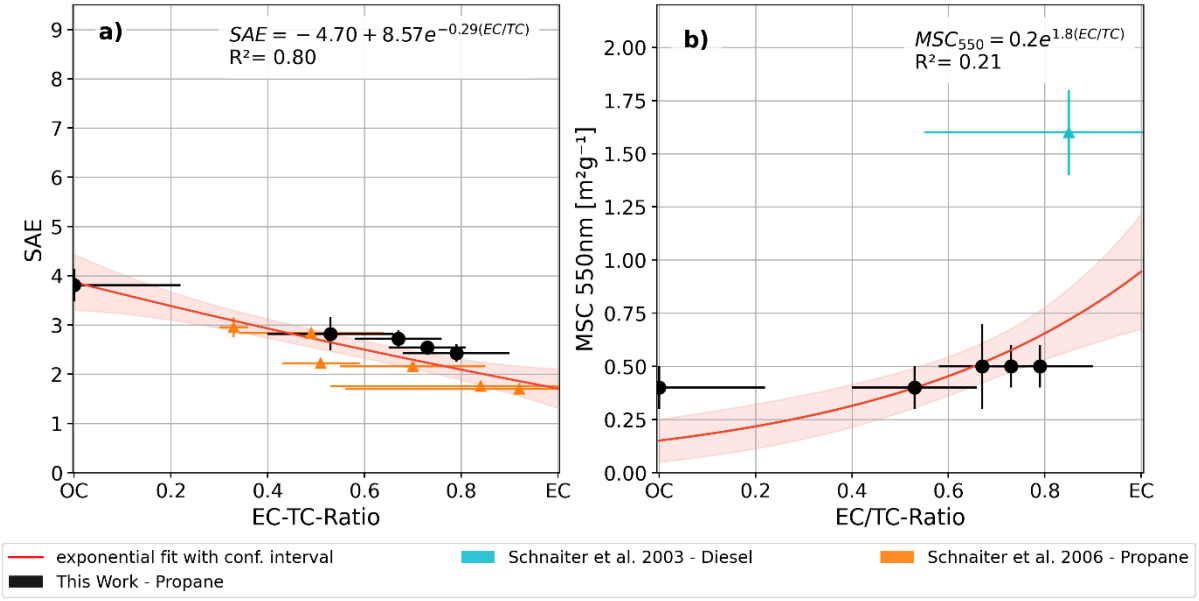

Figure S6. Equivalent plot to Fig. S5, illustrating the results in relation to the EC/OC ratio: Compositional dependent scattering mass scattering cross section and its spectral variability represented by the SAE. The MSC data obtained in the present study at 550 nm (black points) are combined with observations from past literature and put in relation to the EC/OC soot content. Data retrieved as described for Fig.6. The EC/OC ratios, if not available from the original publication, were determined using EC+OC=TC assumption, thus $\frac{OC}{TC} = 1 - \frac{EC}{TC}$, and $\frac{EC}{OC} = \frac{EC}{TC}\frac{TC}{OC}$. In case no uncertainties for EC, OC, or TC were given, the EC/TC uncertainty was assumed to be true for OC/TC and then propagated (resulting in potential underestimations of the EC/OC uncertainty). Please note that these identified relationships have only limited relevance as scattering depends on size.

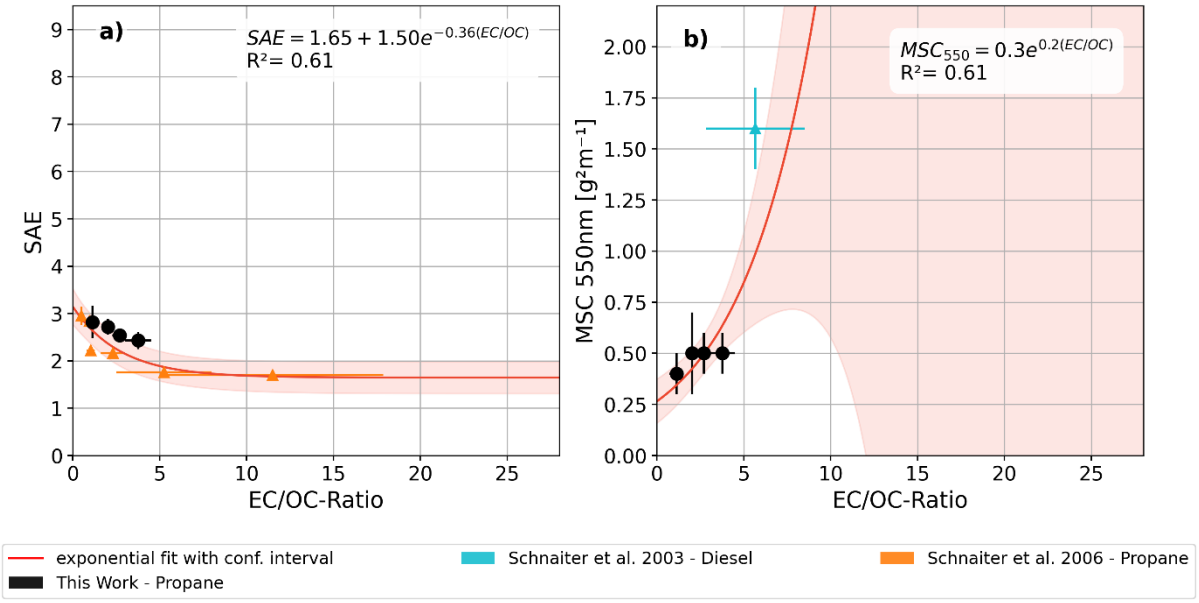

Figure S7. Representative example of the measurements of mass concentration of ammonium sulphate. Comparison of mass concentration in µg m^{-3} from the TEOM (green line) and calculated using the SMPS, assuming spherical particles and using density from the literature (red line; 1.8 g cm^{-3} (e.g. Bond and Bergstrom (2006)) and as measured from the CPMA-system (grey line). The black line marks the beginning of the injection.

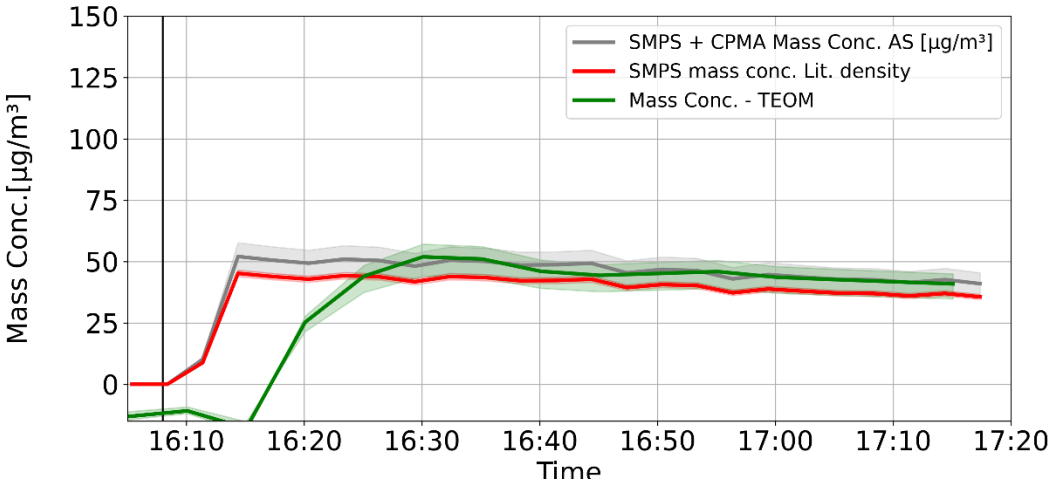

Figure S8. Representative example of the measurements of optical properties of ammonium sulphate experiment. Comparison of the extinction and scattering signals determined at 450 and 630 nm with their uncertainties as shaded areas. The black line marks the injection. Note that the optical instruments are not connected simultaneously and thus differ in their start of measurement.

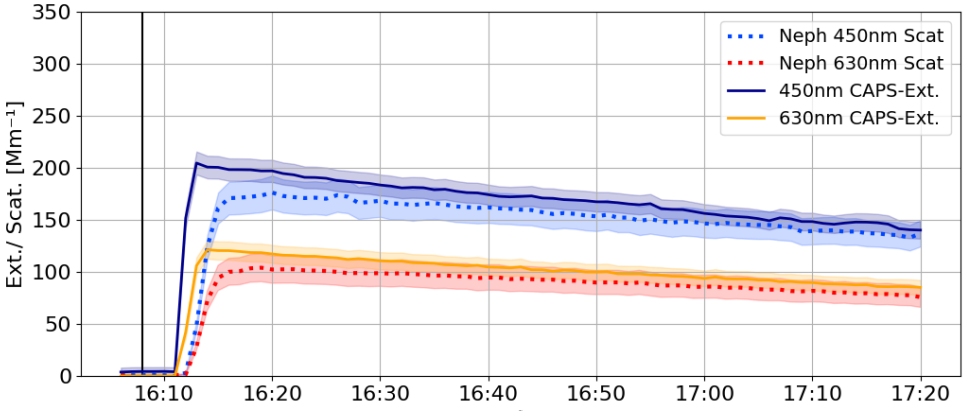

Table S1. Full list of CESAM soot experiments analysed in the present work. Additional information includes the length of the measurement interval for acquisition of the properties of fresh soot (data basis for this paper), total soot lifetime inside the chamber, and initial mass concentration injected into the chamber. Further, the table includes information on additional ageing conditions and injections of different compounds such as water (measured as relative humidity RH), ozone, SO_2, and α-pinene, used to investigate the impact of ageing conditions on soot aerosol properties. These ageing conditions are not considered in the present work.

Experiment	Meas. interval fresh soot (hh:mm)	Total Lifetime (hh:mm)	Initial mass concentration [µg m^{-3}]	RH	O3 [ppb]	SO_2 or α-pinene [ppb]	Date
CS lifetime experiments (dry, dark) – Fresh and aged under the effect of coagulation							
CS1 Lifetime 1	21:51	21:51	63 ± 6	/	/	/	23/02/2021
CS1 Lifetime 2	25:36	25:36	198 ± 18	/	/	/	24/02/2021
CS1 Lifetime 3	05:56	05:56	61 ± 6	/	/	/	19/10/2021
CS2 Lifetime 1	03:05	03:05	99 ± 8	/	/	/	11/03/2021
CS2 Lifetime 2	05:05	05:05	95 ± 8	/	/	/	20/10/2021
CS3 Lifetime 1	01:51	01:51	58 ± 5	/	/	/	11/03/2021
CS3 Lifetime 2	04:32	04:32	89 ± 8	/	/	/	26/10/2021
CS4 Lifetime 1	02:59	02:59	23 ± 2	/	/	/	12/03/2021
CS4 Lifetime 2	06:25	06:25	44 ± 4	/	/	/	22/10/2021
CS5 Lifetime 1	03:53	03:53	46 ± 4	/	/	/	28/05/2021
CS5 Lifetime 2	05:52	05:52	65 ± 7	/	/	/	21/10/2021
CS chemically aged experiments (e.g. 30% RH, light, oxidant)							
CS1 + hv 1	02:56	05:01	67 ± 6	/	/	/	17/05/2021
CS1 + hv 2	01:34	02:37	58 ± 6	/	/	/	19/05/2021
CS1 + H2O	01:55	07:11	78 ± 8	≈ 30%	/	/	26/02/2021
CS1 + H2O + hv	01:32	06:46	79 ± 8	≈ 30%	/	/	01/03/2021
CS1 + O3 + hv	01:42	07:48	74 ± 7	≈ 30%	1345	/	02/03/2021
CS1 + SO2 + hv	01:32	06:50	90 ± 8	≈ 30%	/	272	03/03/2021
CS1 + O3 + SO2 + hv 1	01:37	24:48	89 ± 9	≈ 30%	1437	259	04/03/2021
CS1 + O3 + SO2 + hv 2	02:08	25:16	80 ± 8	≈ 30%	1383	258	09/03/2021
CS1 + O3 + AP	02:01	24:43	63 ± 6	≈ 30%	670	60	18/05/2021
CS1 + O3 + AP - high	02:12	27:03	169 ± 18	≈ 30%	503	120	20/05/2021
CS1 + O3 + AP - low	02:29	07:22	13 ± 2	≈ 30%	559	60	26/05/2021

Table S2. List of key instrumentation used to determine properties of the aerosol particulate phase during the soot experiments in CESAM. Instrument model, measured or derived parameters, time resolution, uncertainty, and main reference or specific data treatment for each technique are provided. For all optical instruments, measurements on HEPA-filter and on the empty chamber were used to determine their current instrumental background noise level, then used to determine the noise-signal-ratio and components of the uncertainty.

Instrument	Measured or derived parameter (units)	Time resolution	Associated Uncertainties		Reference
SMPS System TSI SMPS DMA 3080 & CPC 3772	number size distribution [# cm^{-3}] 19.5 to 881.7 nm	180 s	3% + counting error	Error propagation considering 3% DMA uncertainty in particle mobility size selection plus counting error as the standard deviation of an assumed Poisson distribution	(DeCarlo et al., 2004)
TSI DMA 3080 + CPMA (Cambustion) + CPC 3775 high	P_{eff} (eff. density) [g cm^{-3}] from the mass-resolved number size distribution [# cm^{-3}]	30-45min with 180 s at each mass	10%	Error propagation considering DMA uncertainty, mass-to-charge uncertainty, relative standard error of the size distribution median diameter For mass calculation, the uncertainty in the power law fit under consideration of the eff. density uncertainties is used	Olfert and Collings (2005) With setup as described by Yon et al. (2015)
TEOM 1400a Thermo Scientific	mass concentration [µg m^{-3}]	300 s	15%	Determined on noise operating on chamber using (determined on clean chamber values and as following smoothed variability)	
CPC 3775 TSI	particle number (> 4 nm) [# cm^{-3}]	1 s	10%	associated uncertainties inside the CESAM system	
SP2 Droplet Measurement Technologies (DMT)	Refractory BC (rBC) mass concentration [µg m^{-3}] rBC number size distribution [# cm^{-3}]	60 s	17%	following the observations by Laborde et al. (2012)	Stephens et al., (2003)

Integrating Nephelometer 3563 TSI	scattering coef. [Mm^{-1}] at 450, 550 & 700 nm	1 s	8%	Propagation of uncertainties from cross-calibration (against freshly calibrated Nephelometer), truncation correction, and signal-to-noise ratio (averaged for different total loss conditions)	Description in Anderson et al. (1996) Trunc. corrected using Massoli et al. (2009)
CAPS PM_{ex} Aerodyne	extinction coef. [Mm^{-1}] 2 inst. = 2 wavelength (450, 630nm)	1 s	5-6%	Propagation of uncertainties for general measurement precision (3%, Massoli et al., 2010) and signal-to-noise ratio (averaged for different total loss conditions)	Kebabian et al. (2007) & Massoli et al. (2010)
CAPS PM_{SSA} Aerodyne	extinction coef. [Mm^{-1}] 2 inst. = 2 wavelength (450, 630nm) (only extinction signal used)	1 s	5-6%	Propagation of uncertainties for general measurement precision and signal-to-noise ratio (see above)	Onasch et al. (2015)
CAPS PM_{ex} Aerodyne / Integrating Nephelometer 3563 TSI	absorption coef. [Mm^{-1}] 2 inst. = 2 wavelength (450, 630nm) (extinction minus scattering)	1 s	10-30%	Propagation of uncertainties from the measurements of scattering and absorption including the uncertainties from the interpolation of the scattering signal to 630 nm	
MAAP Thermo-Scientific	absorption coef. [Mm^{-1}] at 637 nm wavelength	60 s	12%	Provided in instruments literature	Petzold and Schönlinner (2004) & Petzold et al. (2005)
TOF - ACSM Aerodyne Research	non-refractory aerosol composition [$\mu g\ m^{-3}$]	360 s	up to 40% (Strongly varying for experiments)	Uncertainty determined from averaged standard deviations of clean air measurements and the intensity of the signal	

Aethalometer (AE33 – dual spot) Magee Scientific	absorption coefficient [Mm^{-1}] 370, 470, 520, 590, 660, 880, 950 nm	60 s	12%	Propagation of uncertainty in Pattenuation (following Backman et al. (2017) and using clean air measurements), the Cref, and the loading correction	Drinovec et al. (2015)
MWAA (Multi-Wavelength Absorbance Analyser)	Abs. coef. [Mm^{-1}] at 375, 405, 532, 635, 850 nm	15-120 min	mean - 19%	Provided by Massabò and team (var. based on filter loading)	Massabò et al. (2013)
PP_UniMI (Polar photometer)	Abs. coef. [Mm^{-1}] at 405, 448, 532, 635, 780 nm	15-120 min	mean - 14%	Provided by Vecchi and team (var. based on filter loading)	Vecchi et al. (2014)
OCEC Carbon Aerosol Analyzer Sunset Laboratory	elemental carbon organic carbon mass concentration [$\mu g\ cm^{-2}$]	5 sec to 240 min	14%/19%/ 18% average for EC/OC/TC	Uncertainties are determined inside the VBasic-Version OCEC835 analysis software for each thermogram and then propagated	EUSAAR protocol Cavalli et al. (2010)
TEM	morphology	30 sec to 120 min		for D_{pp}, D_f, and k_f as output from Bescond et al. (2014) used average is determined using a single determination of all CS1 pictures	

Table S3. List of instrumentation used to characterise the gas phase during the soot experiments in CESAM. Instrument model, measured parameters, time resolution, accuracy, and detection limit of data are given.

Instrument	**Parameter (units)**	**Acquisition resolution (averaged to 1 min)**	**Accuracy (at 1 min time resolution) & detection limit (Acc./DL)**
NO_x Monitor – Horiba APNA370	NO, NO_2 (NOx) [ppb]	5 s	1 / 0.5 ppb
APEE - ProCeas	CO/CO_2 [ppm]	45 s	0.1/ 0.05 ppm
SO_2 Monitor - Horiba APSA370	SO_2 [ppb]	5 s	1/ 0.05 ppb
Ozone (O_3) Monitor - Horiba APOA370	O_3 [ppb]	5 s	1 / 0.05 ppb
Teledyne T500U	NO_2 [ppb]	30 s	0.5% (above 5 ppb)/ 0.04 ppb
Hygrometer - Vaisala HMP234	RH [%] & T [°C]	1 s	2% & ± 0.1 °C (only Acc.)
Baratron type MKS 626AX13TDE (high)/ 626AX11TDE (low)	Pressure [mBar]	1 s	0.25% for 1 to 1000 Torr (Unc.)
PTR-ToF-MS (Kore ltd.)	Mass-loading gaseous components [ppb]	60 s	0.1 ppb [DL]

Table S4. Fitting parameters and values for EC/TC-fit of Fig.6. Fitting parameters correspond to the equation $\boldsymbol{a} * \boldsymbol{e}^{(\boldsymbol{b}*\boldsymbol{EC}/\boldsymbol{TC})}$ for MAC and MSC and $\boldsymbol{a} + \boldsymbol{b} * \boldsymbol{e}^{(-\boldsymbol{c}*\boldsymbol{EC}/\boldsymbol{TC})}$ for AAE and SAE.

		Fitting parameters		
		A	B	C
MAC	Central values	1.3	1.8	/
	Uncertainty	0.05	0.1	/
AAE	Central values	0.73	3.29	2.32
	Uncertainty	0.12	0.12	0.30
MSC	Central values	0.2	1.8	/
	Uncertainty	0.1	1.0	/
SAE	Central values	-4.70	8.57	0.29
	Uncertainty	49.16	48.64	1.94

Table S5. Fitting parameters and values for OC/TC-fit of Figure S4. Fitting parameters corresponds to the equation $\boldsymbol{a} * \boldsymbol{e}^{(b*OC/TC)}$ for MAC and MSC and $\boldsymbol{a} + \boldsymbol{b} * \boldsymbol{e}^{(-c*OC/TC)}$ for AAE and SAE.

		Fitting parameters		
		A	**B**	**C**
MAC	Central values	1.4	3.4	/
	Uncertainty	0.2	0.4	/
AAE	Central values	1.07	2.47	1.30
	Uncertainty	0.01	0.14	0.13
MSC	Central values	0.3	0.2	/
	Uncertainty	0.1	0.1	/
SAE	Central values	1.65	1.50	0.36
	Uncertainty	0.27	0.37	0.26

Table S6. List of control experiments and key parameters like relative humidity, and the lifetime in the chamber. The mass concentration is calculated using averages of measured densities applied to SMPS measurement

Experiment	**Lifetime in dry conditions (hh:mm)**	**Total Lifetime (hh:mm)**	**Est. Initial mass concentration* [µg m^{-3}]**	**RH**	**Date**
$(NH_4)_2SO_4$ - AS 1	00:42	01:36	80.0	≈ 30%	05/03/2021
$(NH_4)_2SO_4$ - AS 2	01:21	01:21	48.6	<2%	10/03/2021
$(NH_4)_2SO_4$ - AS 3	00:43	00:43	185.3	<2%	18/10/2021
H_2SO_4 – SA 1 *(generated as a secondary aerosol)*	*Generate in a humid environment*	03:21	Peak at 54.9	≈ 30%	08/03/2021

Text S1. Injection of soot aerosols in CESAM

The injection of CS aerosol in CESAM was performed by connecting the miniCAST generator output directly to the chamber through an activated carbon denuder. The flame of the miniCAST was let to stabilize for around 2 to 5 minutes prior to injection. A T-connection was placed at the exit of the miniCAST, whose output flow rate is approximately 7 L min^{-1} for all OP points: one of the T exits was connected to CESAM through an activated carbon denuder (optimized for a flow rate of 3 to 6 L min^{-1}), while the second T exit acted as an exhaust system used for the stabilization period and for the remaining flows during the injection process. Two protocols, that generated soot aerosol with the same properties, were used to inject the soot into the chamber: one where the pressure and compensation of the chamber were adjusted to pull with a constant flow of 5 L min^{-1} while the remaining flow (approximately 2 L min^{-1}) was removed via the exhaust and the second one where the exhaust was closed during injection and the outflow of the miniCAST (7 L min^{-1}) was used to push the aerosol against a slight pressure gradient through the denuder into the chamber. The activated carbon denuder was used to minimize the potential injection of volatile organic compounds from the flame exhaust into the chamber and therefore limit any chemical processing of the CS aerosol after the initial combustion process. All connections between the miniCAST and the chamber are made of half-inch stainless steel tubing. To note that during soot injection some of the aerosol online instrumentation was disconnected to avoid any possible damages due to eventual short pressure changes.

Text S2. Mass concentration measurements for the refractory, non-refractory and total aerosol fraction in CESAM

The measurements of the refractory black carbon particle mass concentration (m_{rBC}) and rBC size distribution between 89 and 567 nm (volume equivalent diameter, D_{ve}) were performed with a single particle soot photometer (SP2 – Droplet Measurement Technologies, sampling flow rate 0.12 L min^{-1}; Stephens et al., 2003) using laser-induced incandescence. The SP2 was calibrated using fullerene and size- and mass-selected CS from the miniCAST (following Laborde et al. (2012)) and analysed assuming a material density of 1.8 g cm^{-3}. The measured size distributions were extrapolated based on a lognormal fit in order to approximate the rBC-mass concentrations over the full size range (Liu et al., 2014).

The mass concentration of non-refractory chemical components ($m_{non\text{-}refr}$) including nitrate, sulphate, ammonium, chloride, and organics were measured using a time-of-flight aerosol chemical speciation monitor (TOF-ACSM-Aerodyne, sampling flow rate 1 L min^{-1}) at 6-min resolution and a vaporizer temperature at around 600 °C. The instrument was calibrated with monodispersed ammonium nitrate and ammonium sulphate particles and data were extracted by assuming a collection efficiency of 1.

The total aerosol mass concentration (m_{total}) was determined at a 3 minute the SMPS plus effective density measurement, as described in the main manuscript, and additionally monitored online at 5 minute resolution by means of a tapered element oscillating microbalance (TEOM 1400a – Thermo Scientific, sampling flow rate 3 L min^{-1}) maintained at 300 K. Due to the TEOM sensitivity to even slight pressure changes and potential consequential data instability, its data was mainly used to validate mass calculations from complimentary approaches described.

Text S3. Filter-based aerosol absorption coefficient measurements in CESAM

The absorption coefficient (b_{abs}) at 450 and 630 nm was derived from online measurements throughout each experiment as the difference between b_{ext} and b_{sca} (extinction-minus-scattering approach, EMS) from the CAPS monitors and the nephelometer. Three filter-based techniques for absorption measurements were applied in order to complement and validate the b_{abs} retrieved online by EMS: the Multi Angle Absorption Photometer (MAAP; Petzold et al., 2005; Petzold & Schönlinner, 2004), the Multi-Wavelength Absorbance Analyzer (MWAA; Massabò et al., 2013, 2015), and the polar photometer of the University of Milano (PP_UniMI; Bernardoni et al., 2017; Vecchi et al. 2014). The basic principle of these techniques is the same and based on the MAAP concept. The instruments measure both the transmittance through an aerosol loaded-filter matrix as well as the reflectance at different angles (130° and 165° for the MAAP, 125° and 165° for the MWAA, and between 0 and 170° at an angular resolution of 0.4° for the PP_UniMI). Together with a radiative transfer scheme based on the Mie theory and a two-stream approximation, the measurements of transmitted and reflected light intensity are used to determine the aerosol absorption coefficient. The main advantage of the MAAP, MWAA and PP_UniMI is that b_{abs} is retrieved without the need to correct for the typical artefacts of filter-based techniques like the aethalometer, as the multiple scattering in the filter fiber and the scattering effect by aerosols are taken into account in their radiative transfer scheme.

The key differences between MAAP, MWAA, and PP_UniMI are the operating wavelengths and the deployment mode, therefore determining a different temporal resolution and set up for CESAM experiments:

- The MAAP is a single-wavelength field–deployable instrument operating at 637 nm and typically 1-min resolution. The MAAP was connected online to CESAM during experiments. However, because of its high flow rate (typically of 16.7 L min^{-1}, but reduced to 8 L min^{-1} for the chamber experiments), it was used to measure soot absorption only at specific moments, i.e. shortly after injection in CESAM and towards the end of each experiment, for time intervals ranging between 30 minutes to a maximum of 4 hours.
- The MWAA and the PP_UniMI are laboratory–based setup operating at 5 wavelengths (375, 405, 532, 635, 850 nm for the MWAA and 405, 448, 532, 635, 780 nm for the PP_UniMI). The MWAA and the PP_UniMI work offline with aerosol collected on filter samples, therefore they integrate observations across a sampling period that can be variable depending on the concentrations (minutes to hours). In the present study, the filter tape from the MAAP (Glass filter fiber GF 10) was cut and removed after each measurement interval in CESAM so that the collected filtered spot could serve as the filter samples for the MWAA and PP_UniMI. Filters were stored in a freezer at -20 °C in-between sampling and measurement. Blank filters were taken to evaluate possible artefacts in the observations.

To note that these filter-based techniques, despite being assumed as a reference, can also be affected by a loading effect artefact, i.e. the accumulation of particles on the filter reduces the linearity in the retrieved absorption signal, therefore causing an underestimate of the absorption coefficient for increasing aerosol deposition. For the MAAP, as detailed in (Hyvärinen et al., 2013), this happens when the accumulation rate is higher than 0.04 µg min^{-1}. In this study, when relevant,

the b_{abs} from the MAAP was corrected for the loading effect following the formulation proposed by (Hyvärinen et al., 2013) based on the use of the measured raw reflected signal at 165°. The MWAA and the PP_UniMI results were not corrected for loading effects based on previous intercomparisons between these instruments and Hyvärinen-corrected MAAP data. These intercomparisons indicate that for the given conditions of the absorbance of the filter sample (ABS < 1, i.e. the optical depth of the particle-loaded filter) no need for further corrections exists.

Together with the MAAP, MWAA, and PP_UniMI, filter–based measurements of spectral absorption was performed by aethalometers connected to CESAM online throughout experiments, including both a single-spot AE31 model (Weingartner et al., 2003) and a dual-spot AE33 (Drinovec et al., 2015). Due to the high aerosol loading effects during soot experiments, as well as the uncertainty on the multiple scattering corrections, data from these instruments are not used in the present analysis. However, data from present experiments will be used to study the multiple scattering corrections and performances of the aethalometer for highly absorbing aerosols (Renzi et al., in preparation).

Text S4. Extraction procedure and HPLC-UVVis-ESI/HRMS measurements

The CS particles collected on quartz-fiber filters were extracted to perform HPLC-UVVis-ESI/HRMS analysis. For the extraction procedure, 3 punches of 16 mm each were taken from the 47 mm filter and sonicated in 3 ml of acetonitrile (Fujifilm Wako pure chemical, code: 012-19851, Lot no. ACN 3706). Sonication was performed at 500 rpm for 1h (IKA VIBRAX VXR basic). In order to minimize the exposure to ambient light and so photo-induced reactions during sonication the glass tubes containing the filter samples were covered with aluminium foil. The liquid extracts were then filtered via a PTFE 13 mm-diameter 0.22 mm pore syringe filter (Membrane Solutions) to remove insoluble components and transferred into a glass tube. The resulting solutions were first evaporated (centrifugation at a pressure of 10 kPa at 25°C for about 3 hours; EYELA CVE 2200). Next, 100 µL of acetonitrile was added to get a concentrated solution for HPLC analysis. The obtained solution was homogenized by passing it in an ultrasonic bath for a few seconds. Amber HPLC vials were used to store the solution, which was kept in a freezer at -20°C until analyses. Visual inspection of the filters after acetonitrile extraction indicated remaining material on the filter. This material, mostly of black colour, was assimilable to the remaining insoluble BC on the filters. However, in order to evaluate the presence of any remaining soluble material, sequential extraction in methanol (Fujifilm Wako pure chemical, code: 134-14523, Lot no. TPL 5393) was performed on dried filters for CS1, CS3, and CS5 soot following the same procedure as for acetonitrile extraction. Between extraction and HPLC measurements, the solutions were stored in a freezer.

The analysis of samples was conducted using a High Performance Liquid Chromatography (HPLC; Agilent 1260 infinity) system coupled with a photodiode array (PDA, 190−640 nm, 2 nm resolution) spectrophotometer and a high-resolution mass spectrometer (JEOL JMS-T100LP AccuTOF LC-plus, electrospray ionization high-resolution time-of-flight mass spectrometer; ESI−HRTOFMS) to examine the chemical composition of aerosols. The HPLC separation was carried out on a

Proshell 120, EC-C18 column, 3.0 × 50 mm, with 2.7 μm particle sizes and 120 Å pores, with the temperature set to 30 °C at a flow rate of 0.2 mL/min. The mobile phase consisted of water (eluent A; purification by MilliQ) containing 0.1% formic acid and acetonitrile (eluent B; Fujifilm Wako pure chemical, code: 012-19851, Lot no. ACN 3706). The gradient elution was programmed as follows: 0−5 min 99% eluent A and 1% eluent B; 5−16 min linear ramp to 100% eluent B; 16−24 min hold at 100% eluent B; 24−25 min return to 99% eluent A and 1% eluent B; 25−39 min hold at 99% eluent A and 1% eluent B. The analysis ends at 30 min. The mass spectrometer was operated with a spray voltage of -2 kV and a resolving power of $m/\Delta m$ = 6000. Analysis was done both in negative and positive ion mode. The HPLC−UV/Vis−ESI/HRMS measurement sequence was the following: first only mobile phase without injection is measured, then only acetonitrile pure solution, followed by blanc sample and the CS1 to CS5 samples sequentially.

The obtained UV-Vis absorbance spectra (Abs(λ)) are treated as follows. First, the raw spectra of both pure solvent (acetonitrile, methanol) and sample are referenced to measurements between 620 and 640 nm, a region assumed to be free of absorption:

$$Abs_{sample}(\lambda) = Abs_{sample-raw}(\lambda) - Abs_{sample-raw}(620-640\,nm) \quad \text{(S1)}$$

$$Abs_{solvent}(\lambda) = Abs_{solvent-raw}(\lambda) - Abs_{solvent-raw}(620-640\,nm) \quad \text{(S2)}$$

This baseline correction is done to correct for any possible instrumental drift potentially affecting the signal. The solvent absorbance is then subtracted from the sample signal to isolate the signatures of the elute, as:

$$Abs_{sample-elute}(\lambda) = Abs_{sample}(\lambda) - Abs_{solvent}(\lambda) \quad \text{(S3)}$$

For CS1, CS3, and CS5 for which both acetonitrile and methanol extractions are performed, the total absorbance is calculated as the sum of the two. Nonetheless, absorbance from methanol counts for less than 20% of total absorption and results are shown for the acetonitrile extracts only.

Text S5. Control experiments

Four control experiments were performed using ammonium sulphate (AS - $(NH_4)_2SO_4$) and sulfuric acid (SA - H_2SO_4) to validate and characterize the instrumentational setup, in particular, the optical instrumentation and the mass concentration dataset. Both compounds are largely available atmospheric components and therefore the physico-chemical properties including spectral optical properties have been intensively studied (e.g. Toon et al., 1976; Flores et al., 2009), in particular also inside the CESAM chamber system (e.g. Denjean et al., 2014). The aerosols are considered to be more or less spherical and non-absorbing, which are key properties for the validation of the optical properties as they fit well with the approximation of spherical homogeneous particles for Mie calculations. The non-absorption properties were used to verify that the measured values from the EMS devices agree, meaning $b_{scat}=b_{ext}$ and consequently b_{abs} equals zero.

The ammonium sulphate aerosol was generated from a 0.03M solution (ultrapure water, ≤3.0 ppb of TOC, and Ammonium sulfate, 99.9999% Suprapur®, Merck) using a constant-output atomizer (Model 3076, TSI) operated at a flow rate of 2 L

min^{-1}. The sulfuric acid aerosol was generated by injecting SO_2 (about 270 ppb) in an O_3-rich (1 ppm) humid (>30%) environment and afterwards starting the photo-chemical generation of OH by adding the radiation using three 6.5 kW-xenon-arc lamps through three quartz windows with 6.5 mm-thick Pyrex® filters.

The number size distribution measurements from the SMPS allowed indirect determination of the theoretical extinction and scattering coefficients using Mie theory calculations and refractive indexes assumed from the literature. For spherical particles, as we consider for AS and SA, the mobility diameter of the SMPS can be assimilated to a volume-equivalent diameter (i.e., shape factor equal to 1). On the other hand, Mie calculations can be also used to provide an inverse determination of the refractive index of the aerosol: starting from the measured number distribution and scattering and extinction coefficients, the refractive index of the aerosol can be determined as the value that allows to most closely reproduce the measured optical signals. Mie calculations were done at 3 wavelengths (450, 550, 630 nm) using the b_{scat}, b_{ext}, and b_{abs} from the EMS methods and using extrapolation based on $b_{ext,550} = b_{ext,\lambda_1} * (\frac{\lambda_1}{550})^{AEE_{approx}}$ with $AEE_{approx} = -\frac{\log(\frac{MAC_{\lambda_1}}{MAC_{\lambda_2}})}{\log(\frac{\lambda_1}{\lambda_2})}$ to approximate the extinction at 550 nm and the scattering at 630 nm from the measurements. The SPMS number size distribution together with scans of the DMA-CPMA-CPC system and data from the TEOM, as described in the main manuscript, were additionally used to test and verify the effective density measurements to compare them against available values in literature and check the consistency of mass concentration measurements.

Effective density measurements. The measurements of the effective densities of AS and SA on average were 1.89 ± 0.19 g cm-3 and 1.64 ± 0.16 g cm-3 (size-independent). These values were found to deviate, but still to agree within uncertainties, from the expected values of 1.76 and 1.8 g cm-3 (Hand and Kreidenweis, 2002; Myhre et al., 1998; Tang, 1996) proposed in the literature for the pure and dry compounds. To note however that CESAM values were measured in a humid environment, a condition possibly affecting the aerosol density. For the sulphuric acid in particular the influence of the >30% relative humidity in the chamber reduces the effective density of the aerosol due to the dilution of the acid by the water content in the chamber (Peng et al., 2022), with expected reduction of the density to values around than 1.68-1.7 g cm-3 (Myhre et al., 1998). These results suggest precision and repeatability of the effective density measurements within the provided uncertainty of around 10%.

Mass concentration. Ammonium sulphate experiments were used as key experiments to validate mass concentration measurement by comparing the masses calculated with the SMPS using both the CPMA-measured effective density and the literature density against the mass measured with the TEOM (see Fig. S7). The comparison indicates a very good agreement in mass concentration measurements between the two techniques, with a better agreement when CPMA-derived effective density, instead of the literature values, is used to calculate the mass concentration from number distribution data.

Optical properties. Figure S8 shows the scattering and extinction coefficients for the ammonium sulphate experiment coded as $(NH4)_2SO4$ - AS 2 (dry conditions). The comparison shows that the nephelometer scattering and the CAPS extinction signals, both at 450 and 630 nm agree within their measurement uncertainty, supporting the consistency of measurements.

Despite these observations, a slight systematic difference in the signals of extinction and scattering can be noticed that results in a small absorption signal (of the order of 10 Mm^{-1} from the data shown in Fig. S8) for the EMS-techniques. This is however captured inside the given uncertainties of the absorption coefficient. The results are similar for the other experiments including the sulphuric acid and, despite showing a slight experiment-to-experiment variability, the scattering and extinction agree on average within 9% to 19%, for 450 and 630 nm, respectively, with the highest difference observed at 630 nm. For the sulphuric acid control experiments, low signal strength for scattering and extinction, below 4 Mm^{-1} at 630nm, increases the uncertainties and relative differences for the measurements which are thus not considered in this comparison as they are significantly lower than observed conditions.

Optical calculations with Mie theory were performed to retrieve the refractive indexes for AS and SA aerosols. For the ammonium sulphate, a wavelength-independent average complex refractive index of 1.49 (±0.09) + i0.008 (±0.011) was determined at the three wavelengths. While the values of the real part for AS lay inside the expected values of literature, which vary around 1.5 (Denjean et al., 2014; Toon et al., 1976), the imaginary part shows a slightly nonzero value which we attribute to the identified small absorption signal from EMS calculation. For the sulphuric acid a CRI of 1.24 (±0.05) + i0.004 (±0.007) was determined with this showing slightly lower values of the real part than expected from the literature (around 1.36 to 1.4, (Palmer and Williams, 1975), potentially associated to the humidity effect discussed above, and a small non-zero imaginary part.

Summarizing, the control experiments showed that agreement between the different mass measurements is given and that measured effective densities agree within the range of their uncertainties with the literature values. For the optical properties it was shown that the instruments measuring the scattering and extinction despite very well agreeing within their uncertainty, they do not show perfectly equal values, which determine a small but quantifiable absorbing signal for a purely scattering aerosol. While this absorption signal is within measurement uncertainties and therefore not expected to influence the MAC estimates significantly, it can result in a slight bias for the determination of the CRI using optical calculation. Nonetheless, as we expect the CRI of soot to be two orders of magnitude higher than the 0.004-0.008 obtained in control experiments, the impact of this bias is very reduced.

References:

Anderson, T. L., Covert, D. S., Marshall, S. F., Laucks, M. L., Charlson, R. J., Waggoner, A. P., Ogren, J. A., Caldow, R., Holm, R. L., Quant, F. R., Sem, G. J., Wiedensohler, A., Ahlquist, N. A., and Bates, T. S.: Performance Characteristics of a High-Sensitivity, Three-Wavelength, Total Scatter/Backscatter Nephelometer, J. Atmospheric Ocean. Technol., 13, 967–986, https://doi.org/10.1175/1520-0426(1996)013<0967:PCOAHS>2.0.CO;2, 1996.

Backman, J., Schmeisser, L., Virkkula, A., Ogren, J. A., Asmi, E., Starkweather, S., Sharma, S., Eleftheriadis, K., Uttal, T., Jefferson, A., Bergin, M., Makshtas, A., Tunved, P., and Fiebig, M.: On Aethalometer measurement uncertainties and an instrument correction factor for the Arctic, Atmospheric Meas. Tech., 10, 5039–5062, https://doi.org/10.5194/amt-10-5039-2017, 2017.

Bernardoni, V., Valli, G., and Vecchi, R.: Set-up of a multi wavelength polar photometer for off-line absorption coefficient measurements on 1-h resolved aerosol samples, J. Aerosol Sci., 107, 84–93, https://doi.org/10.1016/j.jaerosci.2017.02.009, 2017.

Bescond, A., Yon, J., Ouf, F. X., Ferry, D., Delhaye, D., Gaffié, D., Coppalle, A., and Rozé, C.: Automated Determination of Aggregate Primary Particle Size Distribution by TEM Image Analysis: Application to Soot, Aerosol Sci. Technol., 48, 831–841, https://doi.org/10.1080/02786826.2014.932896, 2014.

Bond, T. C. and Bergstrom, R. W.: Light Absorption by Carbonaceous Particles: An Investigative Review, Aerosol Sci. Technol., 40, 27–67, https://doi.org/10.1080/02786820500421521, 2006.

Cavalli, F., Viana, M., Yttri, K. E., Genberg, J., and Putaud, J.-P.: Toward a standardised thermal-optical protocol for measuring atmospheric organic and elemental carbon: the EUSAAR protocol, Atmospheric Meas. Tech., 3, 79–89, https://doi.org/10.5194/amt-3-79-2010, 2010.

DeCarlo, P. F., Slowik, J. G., Worsnop, D. R., Davidovits, P., and Jimenez, J. L.: Particle Morphology and Density Characterization by Combined Mobility and Aerodynamic Diameter Measurements. Part 1: Theory, Aerosol Sci. Technol., 38, 1185–1205, https://doi.org/10.1080/027868290903907, 2004.

Denjean, C., Formenti, P., Picquet-Varrault, B., Katrib, Y., Pangui, E., Zapf, P., and Doussin, J. F.: A new experimental approach to study the hygroscopic and optical properties of aerosols: application to ammonium sulfate particles, Atmospheric Meas. Tech., 7, 183–197, https://doi.org/10.5194/amt-7-183-2014, 2014.

Drinovec, L., Močnik, G., Zotter, P., Prévôt, A. S. H., Ruckstuhl, C., Coz, E., Rupakheti, M., Sciare, J., Müller, T., Wiedensohler, A., and Hansen, A. D. A.: The “dual-spot” Aethalometer: an improved measurement of aerosol black carbon with real-time loading compensation, Atmospheric Meas. Tech., 8, 1965–1979, https://doi.org/10.5194/amt-8-1965-2015, 2015.

Flores, J. M., Trainic, M., Borrmann, S., and Rudich, Y.: Effective broadband refractive index retrieval by a white light optical particle counter, Phys. Chem. Chem. Phys., 11, 7943, https://doi.org/10.1039/b905292e, 2009.

Hand, J. L. and Kreidenweis, S. M.: A New Method for Retrieving Particle Refractive Index and Effective Density from Aerosol Size Distribution Data, Aerosol Sci. Technol., 36, 1012–1026, https://doi.org/10.1080/02786820290092276, 2002.

Hyvärinen, A.-P., Vakkari, V., Laakso, L., Hooda, R. K., Sharma, V. P., Panwar, T. S., Beukes, J. P., van Zyl, P. G., Josipovic, M., Garland, R. M., Andreae, M. O., Pöschl, U., and Petzold, A.: Correction for a measurement artifact of the Multi-Angle Absorption Photometer (MAAP) at high black carbon mass concentration levels, Atmospheric Meas. Tech., 6, 81–90, https://doi.org/10.5194/amt-6-81-2013, 2013.

Kebabian, P. L., Robinson, W. A., and Freedman, A.: Optical extinction monitor using cw cavity enhanced detection, Rev. Sci. Instrum., 78, 063102, https://doi.org/10.1063/1.2744223, 2007.

Laborde, M., Schnaiter, M., Linke, C., Saathoff, H., Naumann, K.-H., Möhler, O., Berlenz, S., Wagner, U., Taylor, J. W., Liu, D., Flynn, M., Allan, J. D., Coe, H., Heimerl, K., Dahlkötter, F., Weinzierl, B., Wollny, A. G., Zanatta, M., Cozic, J., Laj, P., Hitzenberger, R., Schwarz, J. P., and Gysel, M.: Single Particle Soot Photometer intercomparison at the AIDA chamber, Atmospheric Meas. Tech., 5, 3077–3097, https://doi.org/10.5194/amt-5-3077-2012, 2012.

Liu, D., Allan, J. D., Young, D. E., Coe, H., Beddows, D., Fleming, Z. L., Flynn, M. J., Gallagher, M. W., Harrison, R. M., Lee, J., Prevot, A. S. H., Taylor, J. W., Yin, J., Williams, P. I., and Zotter, P.: Size distribution, mixing state and source apportionment of black carbon aerosol in London during wintertime, Atmospheric Chem. Phys., 14, 10061–10084, https://doi.org/10.5194/acp-14-10061-2014, 2014.

Massabò, D., Bernardoni, V., Bove, M. C., Brunengo, A., Cuccia, E., Piazzalunga, A., Prati, P., Valli, G., and Vecchi, R.: A multi-wavelength optical set-up for the characterization of carbonaceous particulate matter, J. Aerosol Sci., 60, 34–46, https://doi.org/10.1016/j.jaerosci.2013.02.006, 2013.

Massabò, D., Caponi, L., Bernardoni, V., Bove, M. C., Brotto, P., Calzolai, G., Cassola, F., Chiari, M., Fedi, M. E., Fermo, P., Giannoni, M., Lucarelli, F., Nava, S., Piazzalunga, A., Valli, G., Vecchi, R., and Prati, P.: Multi-wavelength optical determination of black and brown carbon in atmospheric aerosols, Atmos. Environ., 108, 1–12, https://doi.org/10.1016/j.atmosenv.2015.02.058, 2015.

Massoli, P., Murphy, D. M., Lack, D. A., Baynard, T., Brock, C. A., and Lovejoy, E. R.: Uncertainty in Light Scattering Measurements by TSI Nephelometer: Results from Laboratory Studies and Implications for Ambient Measurements, Aerosol Sci. Technol., 43, 1064–1074, https://doi.org/10.1080/02786820903156542, 2009.

Massoli, P., Kebabian, P. L., Onasch, T. B., Hills, F. B., and Freedman, A.: Aerosol Light Extinction Measurements by Cavity Attenuated Phase Shift (CAPS) Spectroscopy: Laboratory Validation and Field Deployment of a Compact Aerosol Particle Extinction Monitor, Aerosol Sci. Technol., 44, 428–435, https://doi.org/10.1080/02786821003716599, 2010.

Myhre, C. E. L., Nielsen, C. J., and Saastad, O. W.: Density and Surface Tension of Aqueous H2SO4 at Low Temperature, J. Chem. Eng. Data, 43, 617–622, https://doi.org/10.1021/je980013g, 1998.

Olfert, J. S. and Collings, N.: New method for particle mass classification—the Couette centrifugal particle mass analyzer, J. Aerosol Sci., 36, 1338–1352, https://doi.org/10.1016/j.jaerosci.2005.03.006, 2005.

Onasch, T. B., Massoli, P., Kebabian, P. L., Hills, F. B., Bacon, F. W., and Freedman, A.: Single Scattering Albedo Monitor for Airborne Particulates, Aerosol Sci. Technol., 49, 267–279, https://doi.org/10.1080/02786826.2015.1022248, 2015.

Palmer, K. F. and Williams, D.: Optical Constants of Sulfuric Acid; Application to the Clouds of Venus?, Appl. Opt., 14, 208, https://doi.org/10.1364/AO.14.000208, 1975.

Peng, C., Chen, L., and Tang, M.: A database for deliquescence and efflorescence relative humidities of compounds with atmospheric relevance, Fundam. Res., 2, 578–587, https://doi.org/10.1016/j.fmre.2021.11.021, 2022.

Petzold, A. and Schönlinner, M.: Multi-angle absorption photometry—a new method for the measurement of aerosol light absorption and atmospheric black carbon, J. Aerosol Sci., 35, 421–441, https://doi.org/10.1016/j.jaerosci.2003.09.005, 2004.

Petzold, A., Schloesser, H., Sheridan, P. J., Arnott, W. P., Ogren, J. A., and Virkkula, A.: Evaluation of Multiangle Absorption Photometry for Measuring Aerosol Light Absorption, Aerosol Sci. Technol., 39, 40–51, https://doi.org/10.1080/027868290901945, 2005.

Stephens, M., Turner, N., and Sandberg, J.: Particle identification by laser-induced incandescence in a solid-state laser cavity, Appl. Opt., 42, 3726, https://doi.org/10.1364/AO.42.003726, 2003.

Tang, I. N.: Chemical and size effects of hygroscopic aerosols on light scattering coefficients, J. Geophys. Res. Atmospheres, 101, 19245–19250, https://doi.org/10.1029/96JD03003, 1996.

Toon, O. B., Pollack, J. B., and Khare, B. N.: The optical constants of several atmospheric aerosol species: Ammonium sulfate, aluminum oxide, and sodium chloride, J. Geophys. Res., 81, 5733–5748, https://doi.org/10.1029/JC081i033p05733, 1976.

Vecchi, R., Bernardoni, V., Paganelli, C., and Valli, G.: A filter-based light-absorption measurement with polar photometer: Effects of sampling artefacts from organic carbon, J. Aerosol Sci., 70, 15–25, https://doi.org/10.1016/j.jaerosci.2013.12.012, 2014.

Weingartner, E., Saathoff, H., Schnaiter, M., Streit, N., Bitnar, B., and Baltensperger, U.: Absorption of light by soot particles: determination of the absorption coefficient by means of aethalometers, J. Aerosol Sci., 34, 1445–1463, https://doi.org/10.1016/S0021-8502(03)00359-8, 2003.

Yon, J., Bescond, A., and Ouf, F.-X.: A simple semi-empirical model for effective density measurements of fractal aggregates, J. Aerosol Sci., 87, 28–37, https://doi.org/10.1016/j.jaerosci.2015.05.003, 2015.